

Capturing Video Frame Rate Variations through Entropic Differencing

Pavan C. Madhusudana
 The University of Texas at Austin
 Austin, TX, USA
 pavancm@utexas.edu

Neil Birkbeck
 Google Inc.
 Mountain View, CA, USA
 birkbeck@google.com

Yilin Wang
 Google Inc.
 Mountain View, CA, USA
 yilin@google.com

Balu Adsumilli
 Google Inc.
 Mountain View, CA, USA
 badsumilli@google.com

Alan C. Bovik
 The University of Texas at Austin
 Austin, TX, USA
 bovik@ece.utexas.edu

ABSTRACT

High frame rate videos are increasingly getting popular in recent years majorly driven by strong requirements by the entertainment and streaming industries to provide high quality of experiences to consumers. To achieve the best trade-off between the bandwidth requirements and video quality in terms of frame rate adaptation, it is imperative to understand the effects of frame rate on video quality. In this direction, we make two contributions: firstly we design a High Frame Rate (HFR) video database consisting of 480 videos and around 19,000 human quality ratings. We then devise a novel statistical entropic differencing method based on Generalized Gaussian Distribution model in spatial and temporal band-pass domain, which measures the difference in quality between the reference and distorted videos. The proposed design is highly generalizable and can be employed when the reference and distorted sequences have different frame rates, without any need of temporal upsampling. We show through extensive experiments that our model correlates very well with subjective scores in the HFR database and achieves state of the art performance when compared with existing methodologies.

KEYWORDS

high frame rate, video quality assessment, full reference, entropy, natural video statistics, generalized Gaussian distribution

1 INTRODUCTION

As current media technology continues to emphasize ever higher quality regimes and to involve more immersive and engaging experiences for consumers, the need to extend current video parameter spaces along spatial and temporal resolutions, screen sizes and dynamic range has become a topic of extreme importance, especially in the media and streaming industry. Existing and emerging standards have increasingly focused on improving spatial resolution (4K/8K) [13], High Dynamic Range (HDR) [16, 21] and multiview formats [10, 36]. However there has been much less emphasis placed on increasing frame rates, and for a long time the frame rates associated with television, cinema and other video streaming applications have changed little - rarely above 60 frames per second (fps).

Various factors have limited increased adoptions of High Frame Rate (HFR) videos. Switching to HFR requires employing complex

capture and display technologies which were not commonly available. However with the development of advanced digital cameras such as GoPro [3], Sony RX series [4], and widespread availability of high performance monitors such as Acer Predator [1], which are primarily designed for gaming applications, HFR technology is well poised for general adoption. Another possible reason for the limited popularity of HFR relates to the limited knowledge about the perceptual benefits of employing HFR, which partly arises due to insufficient availability of HFR content. Recently, HFR domain has gathered significant interest among the research community with publication of databases such as Waterloo HFR [27], BVI-HFR [20] that exclusively target HFR contents.

Before future video pipelines are able to exploit HFR formats, it is imperative to analyze and evaluate the perceptual benefits of using HFR videos. A natural question arises as to whether viewing a particular video at a higher frame rate is better than viewing its lower frame rate version. What is the quality gain that is achievable by going from lower to higher frame rate? This work tries to address these concerns by analyzing subjective quality as well as designing an objective video quality index that seeks to accurately quantify the quality variations that occur due to frame rate variations.

Perceptual Video Quality Assessment (VQA) is an integral component in numerous video applications such as digital cinema, video streaming applications (such as YouTube, Netflix, Hulu etc.) and social media (Facebook, Instagram etc). VQA models can be broadly classified into three main categories [7]: Full-Reference (FR), Reduced-Reference (RR) and No-Reference (NR) models. FR VQA models require entire pristine undistorted stimuli along with degraded versions [22, 33, 35, 41, 45, 47, 49], while RR models operate with limited reference information [5, 17, 37, 38, 44]. NR models operate without any knowledge of pristine stimuli [18, 23, 24, 32]. This work addresses the problem of quality evaluation when pristine and distorted sequences can possibly have different frame rates, thus our primary focus will be on FR and RR VQA methods.

It is a common belief that HFR videos can provide better visual quality, reduction in flicker and motion blur particularly on contents involving high motion. However limited progress on HFR VQA models is making it hard to analyze the actual perceptual gain associated with switching to HFR domain. Although a large number of FR-VQA models have been proposed in the literature, almost all of them require the reference and distorted to have same frame rate since they typically perform pointwise comparisons. Even in

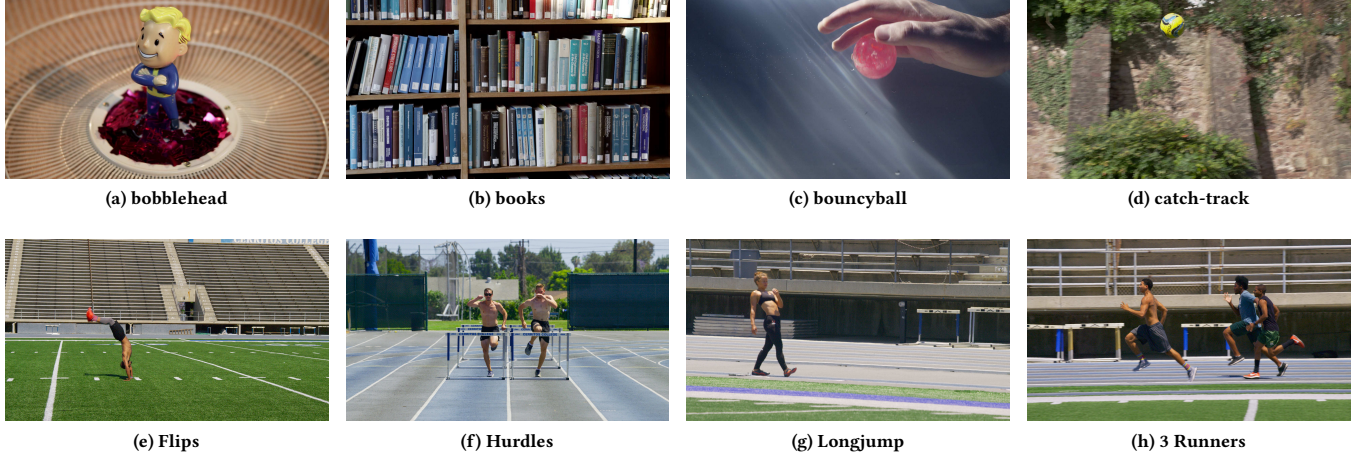


Figure 1: Sample frames from source sequences. (a) - (d): sequences from BVI-HFR and (e) - (h): sequences from Fox Media

RR models, the reduction in reference information occurs mainly along spatial dimensions and not in temporal domain. Although we can apply existing FR/RR methods trivially by upsampling the distorted sequence or downampling the reference, (we assume reference frame rate is always at least as high as that of distorted) we show in our work that this can be counterproductive and can lead to highly inaccurate quality predictions. Moreover upsampling/downsampling process can introduce undesirable artifacts which can potentially affect the accuracy of quality estimates.

There has been very limited work done on addressing VQA in HFR domain. One of the first models was proposed by Nasiri *et al.* [28] where they measured the amount of aliasing occurring in the temporal frequency spectrum and employ that as a measure of quality. In [26] motion smoothness measure is proposed for cross frame rate quality evaluation. Zhang *et al.* [46] propose a wavelet domain based Frame Rate Quality Metric (FRQM), where the difference between wavelet coefficients of reference and temporally upsampled distorted sequence is used to predict quality. FRQM has a limitation that it cannot be employed when both reference and distorted have same frame rate, thus limiting it's generalizability. Moreover all the above methods only account for artifacts arising from frame rate variations, while other artifacts such as compression etc. are not effectively addressed.

Our main contributions are in the design of VQA subjective and objective models that can capture distortions arising due to frame rate variations, and provide quality predictions that correlate well with human perception. Towards this direction our contributions are two fold. Firstly we construct a HFR database consisting of 480 videos and conduct a large scale human study to subjectively evaluate them by obtaining around 40 human opinion scores for each video. This database has unique characteristics since it contains videos upto 120fps and also includes the effects of compression. Although there does exist HFR datasets [20, 27], they either do not consider the impact of compression or only contain videos with ≤ 60 fps. Our second contribution is in the design of a statistical VQA model, which is primarily motivated from variations observed in

the distributions of band-pass coefficients. We propose a novel entropic differencing method using Generalized Gaussian Distribution (GGD) model for both spatial and temporal band-pass responses and show their effectiveness in capturing spatio-temporal artifacts. Our proposed method is simplistic in nature, has very few hyperparameters to tune and does not require any computationally intensive training process. We evaluate our model on the database we develop and show that the predicted quality estimates outperforms existing methods when compared with human opinion scores.

The rest of the paper is organized as follows. In Section 2 we present details about the database construction and subjective study. In Section 3 we provide a detailed description of our proposed VQA model. In Section 4 we report and analyze various experimental results, and provide some concluding remarks in Section 5.

2 SUBJECTIVE QUALITY ASSESSMENT

2.1 Database

We create an HFR database comprised of 480 videos obtained from 16 diverse contents. All the source sequences are natural scenes captured at a frame rate of 120 fps and are currently available in the public domain. Of these 16 contents, 11 were sampled from the Bristol Vision Institute High Frame Rate (BVI-HFR) video database [20], all are of 10 seconds in duration and 1920x1080p (HD) YUV 4:2:0 8 bit format. The other 5 videos correspond to sports content and were captured by Fox Media Group at 3840x2106p (UHD) YUV 4:2:0 10 bit format and 6-8 seconds in duration. Sample video frames presented in the database is shown in Fig. 1.

We created 30 test sequences from each of the source sequences using 6 different frame rates: 24, 30, 60, 82, 98 and 120 fps, and 5 compression levels for each frame rate. The frame rates were chosen based on the refresh rates supported by the monitor (Acer Predator X27 [1]) employed for conducting the human study. All the sequences are compressed using FFmpeg [12] with VP9 [25] compression scheme by varying Constant Rate Factor (CRF) values. The strategy for choosing CRF values was done as follows: 2 values corresponded to lossless (CRF=0) and highest possible compression

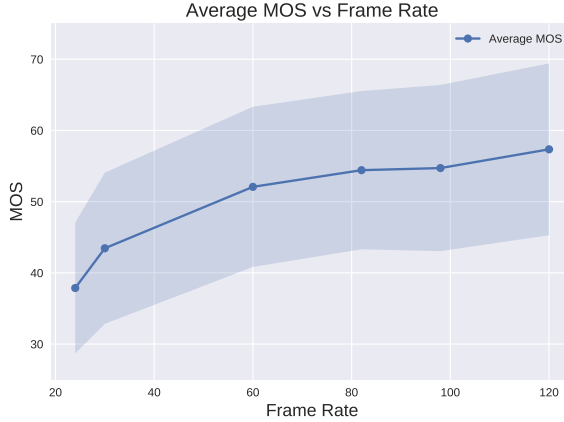


Figure 2: Plot of average MOS across frame rates. The shaded region represents standard deviation ($\pm\sigma$).

level in VP9 (CRF=63), 3 CRF values were chosen such that approximately same bitrate values were obtained across all frame rates for a given source sequence. Thus, for each source content, there are $6(\text{Frame rate}) \times 5(\text{CRF}) = 30$ test sequences. Altogether, there are in total $16 \times 30 = 480$ videos in the database.

2.2 Human Study

We conducted a human study of 85 undergraduate student volunteers at The University of Texas at Austin. The study was of Single-Stimulus Continuous Quality Evaluation (SSCQE) [14] type where the videos were played on Venueplayer [9] application developed by VideoClarity¹. The subjects were provided with a Palette gear console [2] and they could move the cursor over a continuous quality bar press to choose the quality score. The scores were recorded on a scale of 0 to 39, with 39 corresponding to best quality and 0 representing videos suffering from severe distortions. Each subject rated 240 videos across 2 sessions, with each session consisting of 120 videos and lasting approximately 30-40 minutes. A total of 42 human opinion scores were obtained on every video in the database. A subject rejection procedure detailed in the ITU-R BT 500.11 recommendation [14] was used to reject scores from unreliable subjects. In our study nine subjects were rejected and MOS was calculated by averaging scores obtained from the remaining subjects. In Fig. 2 average MOS scores for every frame rate along with their corresponding standard deviation is shown. We observe the effect of diminishing returns with regard to quality perceived and increasing frame rate. Although the quality difference is significant when 24 and 120 fps videos are compared, this gap is much smaller for videos beyond 60 fps. We calculate Difference MOS (DMOS) by subtracting MOS from the corresponding MOS of reference

$$DMOS_i = MOS_i^{ref} - MOS_i \quad (1)$$

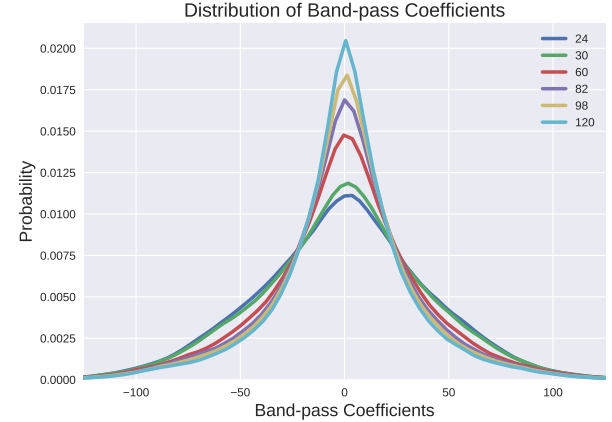


Figure 3: Distribution of band-pass coefficients across different frame rates

3 PROPOSED METHOD

In this section, we introduce a novel FR-VQA method that can be employed when the reference and the distorted videos can possibly have different frame rates. Many existing VQA methods rely on two ideas. One is spatial band-pass filtering such as DCT [32], wavelet decomposition [35, 37, 38] which results in coefficients having a heavy tailed distributions. The second is to apply divisive normalization, based on Gaussian Scale Mixture (GSM) [42] models and the concept of contrast masking. Divisive normalization transform band-pass image coefficients to follow an uncorrelated Gaussian distribution [23, 31]. The presence of distortions tend to disrupt these statistical regularities, thus quality indices try to measure the deviation from the GSM model to quantify quality. Although a large number of VQA models have been proposed in the literature, there has been much less emphasis in designing temporal models to capture temporal artifacts. Existing methods employ basic operations such as absolute temporal differences [19] and frame differences [5, 32, 38] as temporal component in their design. Although they seem to perform well in the general case, their application is restricted to the case where the reference and distorted videos have same frame rate. This work tries to generalize these methods by removing frame rate limitations and accounting for frame rate changes.

Consider a bank of K temporal band-pass filters denoted by b_i for $i \in \{1, \dots, K\}$, the temporal band-pass response for a video $V(\mathbf{x}, t)$ ($\mathbf{x} = (x, y)$ represent spatial co-ordinates and t denotes temporal dimension) is given by

$$B_i(\mathbf{x}, t) = V(\mathbf{x}, t) * b_i(t) \quad \forall i \in 1, \dots, K, \quad (2)$$

where B_i denotes band-pass response of i^{th} filter. Note that these are 1D filters applied only along the temporal dimension. Temporal differences are a special case, where the band-pass filter is essentially the high pass component of a one level Haar wavelet filter. We empirically observe that the distributions of the coefficients of B_i vary as a function of frame rate. This is illustrated in

¹<https://videoclarity.com/>

Fig. 3 where distributions of different frame rates are shown for a 3-level Haar wavelet filter. We observe that as the frame rates increase, the distribution becomes more peaky as the correlation between the consecutive frames increase with frame rate, making band-pass responses more sparse. Our work is primarily motivated from this observation and we extract this deviation to assess quality. Although these band-pass coefficients follow heavy tailed distributions, we observed that application of divisive normalization does not always make their distribution Gaussian.

Although this implies that the coefficients of B_i do not necessarily follow a GSM model, they can be well modelled as following a Generalized Gaussian Distribution (GGD). GGD models have been widely used to model band-pass coefficients in many previous applications such as image denoising [6], texture retrieval [11], Video BLIINDS VQA method [32] etc. Our work is based on the intuition that entropic differences of GGD provide a simplistic way to measure the deviations in distribution of band-pass coefficients occurring due to artifacts arising from changes in frame rate. We leverage on this idea to design a statistical model to capture frame rate variations. In the next subsection we will discuss the GGD based model of band-pass coefficients.

3.1 GGD based statistical model

Let the reference and distorted videos be denoted by R and D respectively, with R_t, D_t representing corresponding frames at time t . Note that R and D can have different frame rates though we require them to have same spatial resolution. Let the response of the i^{th} band pass filter $b_i, i \in \{1, 2, \dots, K\}$ on reference and distorted videos be denoted by B_{it}^R and B_{it}^D respectively. Assume that every frame of B_{it}^R, B_{it}^D follows a GGD model i.e. $B_{it}^R \sim GGD(\mu_{it}^R, \alpha_{it}^R, \beta_{it}^R)$ and $B_{it}^D \sim GGD(\mu_{it}^D, \alpha_{it}^D, \beta_{it}^D)$ where μ is location parameter which is the mean of the distribution, α is a scale parameter and β is the shape parameter. Note that these parameters are time varying depending on the dynamics of the video under consideration. Since the band-pass coefficients have zero-mean, we only consider the two parametric GGD model: $\mu_{it}^R = \mu_{it}^D = 0 \forall i, t$. The probability density expression for a zero mean GGD(α, β) is given by:

$$f(x; \alpha, \beta) = \frac{\beta}{2\alpha\Gamma(1/\beta)} \exp\left(-\left(\frac{|x|}{\alpha}\right)^\beta\right) \quad (3)$$

where $\Gamma(\cdot)$ is the gamma function:

$$\Gamma(a) = \int_0^\infty x^{a-1} e^{-x} dx. \quad (4)$$

The shape parameter β controls the shape of the distribution while α affects the variance. Special cases of GGD include the Gaussian distribution when $\beta = 2$ and Laplacian distribution for $\beta = 1$. Let the band pass coefficients at frame t be partitioned into nonoverlapping blocks of size $\sqrt{M} \times \sqrt{M}$, which are indexed by $b \in \{1, 2, \dots, B\}$. Let B_{ibt}^R and B_{ibt}^D denote vector of band pass coefficients in block b for subband i and frame t for reference and distorted respectively. We allow the band-pass coefficients to pass through a Gaussian channel to model perceptual imperfections such as neural noise [35, 38]. Let $\tilde{B}_{ibt}^R, \tilde{B}_{ibt}^D$ represent coefficients which undergo channel imperfections to obtain the observed responses B_{ibt}^R, B_{ibt}^D respectively. Also let $\tilde{B}_{ibt}^R, \tilde{B}_{ibt}^D$ both be a GGD random variable. This model is

expressed as:

$$B_{ibt}^R = \tilde{B}_{ibt}^R + W_{ibt}^R \quad B_{ibt}^D = \tilde{B}_{ibt}^D + W_{ibt}^D \quad (5)$$

where \tilde{B}_{ibt}^R is independent of W_{ibt}^R , \tilde{B}_{ibt}^D is independent of W_{ibt}^D , $W_{ibt}^R \sim \mathcal{N}(0, \sigma_W^2 \mathbf{I}_M)$ and $W_{ibt}^D \sim \mathcal{N}(0, \sigma_W^2 \mathbf{I}_M)$. It can be inferred from equation 5 that B_{ibt}^R, B_{ibt}^D need not necessarily be GGD, although it can be well approximated by a GGD [48] due to the independence assumption. Similar to [37, 38] we hypothesize that the entropy values of $\tilde{B}_{ibt}^R, \tilde{B}_{ibt}^D$ quantify information pertaining to observed quality variations. The entropy of a GGD random variable $X \sim GGD(0, \alpha, \beta)$ has a closed form expression given by:

$$h(X) = \frac{1}{\beta} - \log\left(\frac{\beta}{2\alpha\Gamma(1/\beta)}\right) \quad (6)$$

Entropy computation requires the values of the GGD parameters of \tilde{B}_{ibt}^R and \tilde{B}_{ibt}^D . However we have access only to B_{ibt}^R and B_{ibt}^D . Thus to estimate these parameters we follow the kurtosis matching procedure detailed in [39]. The first step is to estimate variance, which is a straightforward calculation due to independence assumption

$$\begin{aligned} \sigma^2(B_{ibt}^R) &= \sigma^2(\tilde{B}_{ibt}^R) + \sigma_W^2, & \sigma^2(\tilde{B}_{ibt}^R) &= \sigma^2(B_{ibt}^R) - \sigma_W^2 \\ \sigma^2(B_{ibt}^D) &= \sigma^2(\tilde{B}_{ibt}^D) + \sigma_W^2, & \sigma^2(\tilde{B}_{ibt}^D) &= \sigma^2(B_{ibt}^D) - \sigma_W^2 \end{aligned} \quad (7)$$

The next step is to calculate the kurtosis κ :

$$\kappa(\tilde{B}_{ibt}^R) = \kappa(B_{ibt}^R) \left(\frac{\sigma^2(B_{ibt}^R)}{\sigma^2(\tilde{B}_{ibt}^R)} \right)^2, \quad \kappa(\tilde{B}_{ibt}^D) = \kappa(B_{ibt}^D) \left(\frac{\sigma^2(B_{ibt}^D)}{\sigma^2(\tilde{B}_{ibt}^D)} \right)^2 \quad (8)$$

Interested readers can refer to [29, 39] for a detailed derivation of equation 8. Sample variance and kurtosis values of B_{ibt}^R, B_{ibt}^D are employed in equation 8 to calculate the kurtosis of \tilde{B}_{ibt}^R and \tilde{B}_{ibt}^D respectively. Lastly, the GGD parameters and kurtosis have a bijective mapping [39] where the kurtosis of a GGD random variable is given by:

$$Kurtosis(X) = \frac{\Gamma(5/\beta)\Gamma(1/\beta)}{\Gamma(3/\beta)^2} \quad (9)$$

A simple grid search can be used to estimate the shape parameter β from the kurtosis value obtained from equation 8. The other parameter α can be obtained using the relation

$$\alpha = \sigma \sqrt{\frac{\Gamma(1/\beta)}{\Gamma(3/\beta)}} \quad (10)$$

Plugging the parameters obtained from equations 9 and 10 in 6, the entropies $h(\tilde{B}_{ibt}^R)$ and $h(\tilde{B}_{ibt}^D)$ can be computed. In the next section we show how these entropies can be effectively used to assess the quality of videos.

3.2 Temporal Measure

We define entropy scaling factors given by:

$$\gamma_{ibt}^R = \log(1 + \sigma^2(\tilde{B}_{ibt}^R)), \quad \gamma_{ibt}^D = \log(1 + \sigma^2(\tilde{B}_{ibt}^D)) \quad (11)$$

These scaling factors are similar to the ones used in [37, 38]. Scaling factors lend a more local nature to our model and also provide numerical stability in the regions having low variance as entropy

estimates can be inconsistent in these parts. Entropies are modified by premultiplying these scaling factors to obtain

$$\epsilon_{ibt}^R = \gamma_{ibt}^R h(\tilde{B}_{ibt}^R), \quad \epsilon_{ibt}^D = \gamma_{ibt}^D h(\tilde{B}_{ibt}^D) \quad (12)$$

Although we can simply use the absolute difference between the entropies as a quality measure, there exists a frame rate bias associated with the entropy values where different frame rates have have entropies at different *scales*. Typically high frame rate sequences such as 120fps have much lower entropy values when compared to lower frame rates such as 24fps, 30fps etc. Thus simple subtraction is a measure of the difference between the frame rates of R and D . Though this is desirable, this can be counterproductive when we are comparing two distorted videos which have the same frame rate but different compression levels, as frame rate bias dominates entropy variation arising due to compression. To remove this bias, we employ an additional video sequence termed Pseudo Reference (PR) signal, which is obtained by temporally downsampling the reference to match the frame rate of distorted. We use frame dropping for temporal downsampling, although any other downsampling technique can be employed to accomplish the same. In the case when distorted sequence has the same frame rate as reference, PR will be equal to reference. Similar to B_{ibt}^R and B_{ibt}^D , we calculate ϵ_{ibt}^{PR} . We define the Generalized Temporal Index (GTI) as:

$$GTI_{it} = \frac{1}{B} \sum_{b=1}^B \left| \left(K + |\epsilon_{ibt}^D - \epsilon_{ibt}^{PR}| \right) \frac{\epsilon_{ibt}^R}{\epsilon_{ibt}^{PR}} - K \right| \quad (13)$$

The expression in 13 can be interpreted by decomposing into two factors: absolute difference term and ratio term. Absolute difference term removes frame rate bias and captures the quality changes as if the reference was at the same frame rate. The ratio term weights these factors depending on the reference and distorted frame rate. Note that in the case of same frame rate for reference and distorted, the ratio term will be 1, making the expression in 13 only depend on absolute difference. K is a predefined constant that is used to avoid GTI becoming zero when $D = PR \neq R$, which is the case when distorted video is a downsampled version of the reference, since it can possibly contain temporal artifacts. Note that $GTI = 0$ only when $D = PR = R$. In our implementation we use $K = 1$.

3.3 Spatial Measure

In the previous section we discussed capturing temporal information by using temporal band-pass responses. Although GTI does capture spatial information, it is primarily influenced by the temporal filtering. To address this concern, we employ spatial band-pass filters applied to every frame with the aim of extracting information about spatial artifacts. We use a simple local Mean Subtracted (MS) filtering similar to [5]. Let $R_t^{MS} = R_t - \mu_t^R$ and $D_t^{MS} = D_t - \mu_t^D$ be the reference and distorted MS coefficients where local mean is calculated as

$$\begin{aligned} \mu_t^R(i, j) &= \sum_{g=-G}^G \sum_{h=-H}^H \omega_{g,h} R_t(i+g, j+h), \\ \mu_t^D(i, j) &= \sum_{g=-G}^G \sum_{h=-H}^H \omega_{g,h} D_t(i+g, j+h) \end{aligned} \quad (14)$$

Algorithm 1: Generalized Spatio-Temporal Index

Input: Reference Video R , Distorted Video D

Output: GSTI

- 1 Temporal downsampling to obtain Pseudo Reference (PR)
- 2 Temporal band-pass filtering with b_i , obtain $B_{ibt}^R, B_{ibt}^D, B_{ibt}^{PR}$
- 3 Spatial band-pass filtering, obtain R_{bt}^{MS}, D_{bt}^{MS}
- 4 Calculate $\epsilon_{ibt}^R, \epsilon_{ibt}^D, \epsilon_{ibt}^{PR}$ from equation 12
- 5 Calculate $\theta_{bt}^R, \theta_{bt}^D$ from equation 17
- 6 Temporal entropy pooling from equation 19
- 7 Reference entropy subsampling from equation 23
- 8 Calculate GTI, GSI from equations 13 and 18 respectively
- 9 Obtain $GSTI$ from equation 21

where $\omega = \omega_{g,h}|g = -G, \dots, G, h = -H, \dots, H$ is a 2D circularly symmetric Gaussian weighting function sampled out to 3 standard deviations and rescaled to unit volume and R_t, D_t are frames in pixel domain. In our implementation we use $G = H = 7$. The MS coefficients R_t^{MS}, D_t^{MS} as well follow GGD model. Similar to temporal response, we divide each frame into nonoverlapping blocks of size $\sqrt{M} \times \sqrt{M}$ and index by $b \in \{1, 2, \dots, B\}$. The channel imperfections can be similarly modeled as:

$$R_{bt}^{MS} = \tilde{R}_{bt}^{MS} + Z_{bt}^R \quad D_{bt}^{MS} = \tilde{D}_{bt}^{MS} + Z_{bt}^D \quad (15)$$

where \tilde{R}_{bt}^{MS} is independent of Z_{bt}^R , \tilde{R}_{bt}^{MS} is independent of Z_{bt}^D , $Z_{bt}^R \sim \mathcal{N}(0, \sigma_Z^2 \mathbf{I}_M)$ and $Z_{bt}^D \sim \mathcal{N}(0, \sigma_Z^2 \mathbf{I}_M)$. The entropies $h(\tilde{R}_t^{MS})$ and $h(\tilde{D}_t^{MS})$ can be calculated using the procedure detailed in subsection 3.1 by replacing temporal band-pass responses with corresponding MS coefficients. Similarly we define scaling factors and modified entropies:

$$\eta_{bt}^R = \log(1 + \sigma^2(\tilde{R}_{bt}^{MS})), \quad \eta_{bt}^D = \log(1 + \sigma^2(\tilde{D}_{bt}^{MS})) \quad (16)$$

$$\theta_{bt}^R = \eta_{bt}^R h(\tilde{R}_{bt}^{MS}), \quad \theta_{bt}^D = \eta_{bt}^D h(\tilde{D}_{bt}^{MS}) \quad (17)$$

Since spatial entropies are computed using only the information from a single frame, the values are frame rate agnostic. Thus there does not arise any scale variations due to frame rate bias as seen in the temporal case. The Generalized Spatial Index (GSI) is defined as:

$$GSI_t = \frac{1}{B} \sum_{b=1}^B |\theta_{bt}^D - \theta_{bt}^R| \quad (18)$$

3.4 Temporal Entropy Pooling

Empirically we observe that employing entropy terms obtained from every frame results in noisy quality estimates. The effectiveness of the obtained quality estimates can be greatly enhanced by incorporating a temporal pooling strategy for entropy terms. We consider a window of length L and replace entropy terms at frame

t by averaging a block of consecutive L entropy estimates.

$$\begin{aligned}\epsilon_{ibt}^D &\leftarrow \frac{1}{L} \sum_{t'=t}^{t+L-1} \epsilon_{ibt'}^D, \quad \epsilon_{ibt}^R \leftarrow \frac{1}{L} \sum_{t'=t}^{t+L-1} \epsilon_{ibt'}^R, \quad \epsilon_{ibt}^{PR} \leftarrow \frac{1}{L} \sum_{t'=t}^{t+L-1} \epsilon_{ibt'}^{PR} \\ \theta_{bt}^R &\leftarrow \frac{1}{L} \sum_{t'=t}^{t+L-1} \theta_{bt'}^R, \quad \theta_{bt}^D \leftarrow \frac{1}{L} \sum_{t'=t}^{t+L-1} \theta_{bt'}^D\end{aligned}\quad (19)$$

The pooled entropy terms are then used in equations 13 and 18 to obtain temporal and spatial measure respectively. In our experiments we choose $L = 5$. We discuss the impact of L on performance in section 4.5.

3.5 Spatio-temporal Measure

GSI and GTI operate individually on data obtained by separate processing of spatial and temporal frequency responses. Interestingly, while GSI is obtained in a purely spatial manner, GTI has both spatial and temporal information embedded in it (as entropies are obtained in a spatial blockwise manner). Thus temporal artifacts such as judder etc. only influence GTI, while spatial artifacts affect both GTI and GSI. A combined Generalized Spatio-Temporal Index (GSTI) is defined as:

$$GSTI_{it} = GTI_{it} GSI_t \quad (20)$$

The quality score obtained from equation 20 provides scores at the frame level. To obtain a video level quality score we average pool frame scores:

$$GSTI_i = \frac{1}{T} \sum_{t=1}^T GSTI_{it} \quad (21)$$

3.6 Implementation Details

For simplicity we implement our method only in luminance domain. We use a 3-level Haar wavelet filter as the temporal band-pass filter b_i with $i \in \{1, \dots, 7\}$, (we ignore the low pass response) where higher i value denotes larger center frequency. We use wavelet packet filter [8] as it provides linear bandwidth which is beneficial in analyzing the impact of individual frequency bands on perceived quality. For entropy calculation we choose spatial blocks of size 5×5 (i.e. $\sqrt{M} = 5$). We choose neural noise variance $\sigma_W^2 = \sigma_Z^2 = 0.1$ defined in equations 5 and 15. Note that similar values were employed in [35] and [37]. We observed that our algorithm is most effective when spatial resolution is downsampled 16 times along both dimensions. Similar observations were made in [38] and [5] and is attributed to motion downshifting phenomenon where in presence of motion humans tend to be more sensitive to coarser scales than finer ones. Downsampling also has an additional advantage of reducing computational complexity. Since reference and distorted sequences can have different frame rates, the reference entropy terms $\epsilon_{ibt}^R, \theta_{bt}^R$ will have a different number of frames when compared to their counterpart distorted entropy terms $\epsilon_{ibt}^D, \theta_{bt}^D$. Thus we temporally average reference entropy terms as:

$$k = \frac{FPS_{ref}}{FPS_{dist}} \quad (22)$$

Table 1: Performance comparison across different FR algorithms on the HFR database. In each column first and second best values are marked boldface and underlined, respectively

	SROCC \uparrow	KROCC \uparrow	PLCC \uparrow	RMSE \downarrow
PSNR	0.7062	0.5163	0.6810	9.094
SSIM [49]	0.4717	0.3277	0.4717	10.95
MS-SSIM [45]	0.5082	0.3553	0.4863	10.85
FSIM [47]	0.4556	0.3187	0.4535	11.068
ST-RRED [38]	0.5663	0.3893	0.5298	10.532
SpEED [5]	0.5003	0.3508	0.4631	11.006
FRQM [46]	0.4260	0.2964	0.4453	11.08
VMAF [19]	<u>0.7500</u>	<u>0.5564</u>	<u>0.7288</u>	<u>8.503</u>
deepVQA [15]	0.3575	0.3463	0.2462	11.650
Ours	0.8064	0.6109	0.7973	7.495

$$\tilde{\epsilon}_{ibt}^R = \frac{1}{k} \sum_{n=1}^k \epsilon_{ibt'}^R, \quad \tilde{\theta}_{bt}^R = \frac{1}{k} \sum_{n=1}^k \theta_{bt'}^R \quad \text{where } t' = (t-1)k + n \quad (23)$$

The above procedure is equivalent to dividing the entropy terms into k subsequences along the temporal dimension and averaging each subsequence [20]. The entire algorithm is summarized in Algorithm 1.

4 EXPERIMENTS

In this section we first describe the experimental settings, comparison methods and basic evaluation criteria. Secondly, we evaluate our proposed method against existing state of the art algorithms. Next we perform various ablation studies to analyze the performance variation.

4.1 Experimental Settings

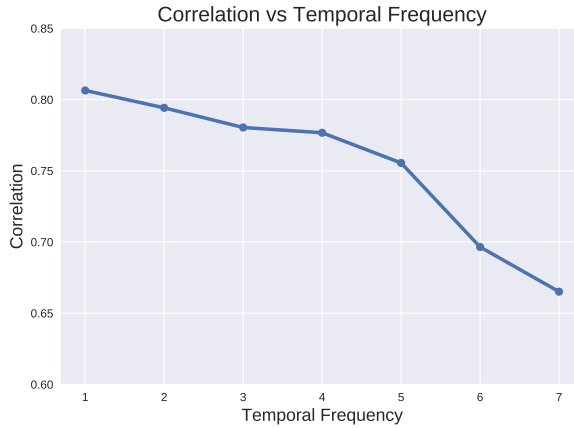
Compared Methods. Since our proposed framework is an FR/RR model, we selected 4 FR-IQA methods: PSNR, SSIM [49], MS-SSIM [45] and FSIM [47] for comparison. Note that these are image indices and do not take into account any temporal information. These indices are computed on every frame and averaged across all frames to obtain the video score. In addition to the above IQA metrics, we also include 5 FR-VQA indices: ST-RRED [38], SpEED [5], FRQM [46], VMAF² [19] and deepVQA [15]. For deepVQA we use only stage-1 of the pretrained model (trained on LIVE-VQA [34] database) obtained from the code released by the authors. All the above methods assume the reference and corresponding distorted sequences to have the same frame rate. For cases with differing frame rates, we perform a naive temporal upsampling by frame duplication to match the reference frame rate. Although we can downsample the reference as well, we avoid this method since it can potentially introduce artifacts (e.g. judder) in reference which is not desirable.

Evaluation Criteria. Spearman’s rank order correlation coefficient (SROCC), Kendall’s rank order correlation coefficient (KROCC), Pearson’s linear correlation coefficient (PLCC) and root mean squared

²we use the pretrained VMAF model available at <https://github.com/Netflix/vmaf>

Table 2: Performance comparison of various FR methods for individual frame rates in the HFR database. In each column first and second best values are marked boldface and underlined, respectively

	24 fps		30 fps		60 fps		82 fps		98 fps		120 fps		Overall	
	SROCC↑	PLCC↑												
PSNR	0.4226	0.3788	0.4849	<u>0.4316</u>	0.6374	0.5880	0.7083	0.6530	0.7311	0.6510	0.6106	0.5987	0.7062	0.6810
SSIM [49]	0.1699	0.1106	0.1834	0.1020	0.2327	0.2048	0.2569	0.2687	0.4142	0.4084	0.7673	0.6926	0.4717	0.4717
MS-SSIM [45]	0.2546	0.1736	0.2595	0.1374	0.2709	0.2119	0.3264	0.2781	0.4447	0.4147	0.6277	0.5987	0.5082	0.4863
FSIM [47]	0.3724	0.3126	0.3516	0.2718	0.2632	0.2678	0.3275	0.3102	0.3895	0.2721	0.3098	0.1129	0.4556	0.4535
ST-RRED [38]	0.1656	0.0718	0.1608	0.0059	0.5103	0.4496	0.3695	0.3548	0.5094	0.4730	0.6808	0.5957	0.5663	0.5298
SpEED [5]	0.2702	0.1478	0.2727	0.1139	0.1888	0.1245	0.3141	0.2593	0.4154	0.3392	0.6929	0.6124	0.5003	0.4631
FRQM [46]	0.1110	0.0105	0.0960	0.0117	0.0912	0.0698	0.0139	0.0102	0.0400	0.0131	-	-	0.4260	0.4453
VMAF [19]	0.2206	0.2953	0.3477	0.3988	0.5681	<u>0.6174</u>	<u>0.7179</u>	<u>0.7589</u>	0.8476	0.8349	0.8030	0.8020	<u>0.7500</u>	<u>0.7288</u>
deepVQA [15]	0.1386	0.0732	0.1846	0.1197	0.2594	0.1698	0.2123	0.1686	0.2825	0.2707	0.6887	0.6301	0.3575	0.3463
Ours	0.4569	0.5872	<u>0.5555</u>	0.6649	<u>0.6349</u>	0.7219	<u>0.7363</u>	0.8064	<u>0.7782</u>	<u>0.7812</u>	<u>0.7649</u>	<u>0.7219</u>	0.8064	<u>0.7973</u>

**Figure 4: Variation of SROCC with temporal frequency bands (b_1, \dots, b_7). X-axis denotes subband index $i \in \{1, \dots, 7\}$**

error (RMSE) are the main performance criteria employed to evaluate VQA methodologies. Before computing PLCC and RMSE, the predicted scores are passed through a four-parameter logistic non-linearity as described in [40]

$$Q(x) = \beta_2 + \frac{\beta_1 - \beta_2}{1 + \exp\left(-\left(\frac{x - \beta_3}{|\beta_4|}\right)\right)} \quad (24)$$

4.2 Correlation with Human Judgments

In this section we analyze the correlation between objective scores predicted by various FR methods against human judgments obtained in the form of DMOS from equation 1. We use uncompressed 120 fps videos (CRF=0) as reference sequences. The performance of various FR methods is shown in Table 1. FR-IQA indices PSNR, SSIM, MS-SSIM and FSIM have poor performance due to absence of temporal information which carries great significance in HFR database. Our proposed method outperforms all the existing models across every evaluation criteria as illustrated in Table 1.

The reported results for our method in Table 1 correspond to the first subband (*i.e.* b_1) of the band-pass filter. In Fig. 4 we plot the performance variation with the choice of b_i , $i \in \{1, \dots, 7\}$ where

Table 3: Significance of Spatial and Temporal Measures

	SROCC↑	KROCC↑	PLCC↑	RMSE↓
Spatial Measure	0.7352	0.5356	0.7096	8.75
Temporal Measure	0.6460	0.4646	0.6466	9.473
Overall	0.8064	0.6109	0.7973	7.495

higher value of i represents higher center-frequency. The degradation in performance for higher frequencies could be explained in terms of temporal contrast sensitivity function (CSF) [30] of human vision, according to which the sensitivity to the visual signal follows a band-pass response, resulting in reduced sensitivity to higher frequencies.

4.3 Performance Analysis with individual frame rates

In this experiment we subdivide the HFR database into sets which contain videos having the same frame rate and individually analyze the performance on them. The performance comparison is shown in Table 2. To avoid clutter we only include SROCC and PLCC for evaluation. KROCC and RMSE as well follow similar trends as shown in Table 2. We observe that our proposed method achieved either first or second best performance across every frame rate. We also observed an interesting anomaly where PSNR achieves higher performance at lower frame rates when compared to other prior perceptual indices. This is counter-intuitive, given that in many prior works PSNR has been shown to correlate poorly with human perception [43]. A possible reasoning behind this observation can be that temporal upsampling by frame duplication artificially boosts PSNR performance. Though the same argument can be made for other perceptual indices like SSIM, MS-SSIM etc., the global nature of PSNR can be a possible factor for this enhancement, differing from local neighborhood based perceptual methods such as SSIM, MS-SSIM etc. Note that at 120 fps, the performance of PSNR is lower than other perceptual IQA indices since there is no frame duplication involved in this evaluation, as reference and distorted are at the same frame rate.

From Table 2 we observe that prediction performance of our method increases gradually with frame rate. This behavior can be explained in terms of frame rate and compression, and their effect on spatial and temporal measures. Note that the frame rate of reference video will always remain same. Fixing the frame rate makes the

Table 4: Performance variation with change in Temporal Pooling Window length

L	SROCC↑	KROCC↑	PLCC↑	RMSE↓
1	0.7730	0.5774	0.7601	8.07
3	0.7990	0.6054	0.7915	7.589
5	0.8064	0.6109	0.7973	7.495
7	0.8055	0.6098	0.7962	7.513
10	0.8058	0.6086	0.7951	7.531
20	0.7937	0.5948	0.7802	7.767

videos only differ by compression levels. Our hypothesis is that in the case of lower frame rates, the temporal measure dominates over spatial measure leading to lower capability of distinction between videos which only differ by compression levels. As the frame rate increases, spatial measure becomes more dominant resulting in higher performance.

4.4 Significance of Spatial and Temporal Measures

To study the impact of each conceptual component present in our algorithm, we test them in isolation and the correlation values are reported in Table 3. It can be inferred from the table that spatial and temporal measure possibly contribute complementary quality information, as their combination yields a higher performance than their respective individual performances.

4.5 Influence of Entropy Temporal Pooling Window

In section 3.4 we introduced temporal pooling of entropy estimates by a window of length L to enhance quality prediction. In Table 4 we show the variation of performance across different choices of window length L . Note that $L = 1$ is equivalent to not performing any pooling operation. We can infer from the table that the performance is not particularly sensitive to the choice of L except for the extreme values.

4.6 Impact of bitrate on Quality Prediction

In the construction of the HFR database we had discussed that the compression levels were chosen such that there were 5 distinct bitrate levels for a given content. We divide the dataset into these 5 sets and their individual performance is shown in Table 5 (the value of bitrates decrease monotonically from bitrate-1 to bitrate-5). We can infer from the table that the qualities predicted in the high bitrate region are more accurate than lower in the lower bitrate regime. This is due to the fact that when bitrate is high, videos only differ by frame rate and the effect of compression is less. Thus it's easier to predict quality since it only depends on the temporal measure. However when bitrate is low, both temporal and spatial measures come into play and their simple product is not particularly effective in capturing this quality variation.

5 CONCLUSION AND FUTURE WORK

We presented a simple, highly generalizable video quality evaluation method that can be employed when reference and distorted

Table 5: Performance variation with Bitrate

	SROCC	KROCC	PLCC	RMSE
Bitrate-1 (Highest)	0.8046	0.5962	0.8467	5.6265
Bitrate - 2	0.8270	0.6285	0.8291	5.434
Bitrate - 3	0.6590	0.4772	0.7005	6.416
Bitrate - 4	0.3415	0.2246	0.3863	8.14
Bitrate - 5 (Lowest)	0.3456	0.2289	0.3217	10.3958

videos having different frame rates, and gauged its performance on our newly designed HFR database. An important characteristic of our method is that it captures spatio-temporal artifacts by means of spatial and temporal measures with no requirement of any temporal upsampling. We performed a holistic evaluation of our method in terms of correlation with human perception and established that our method is superior and more robust than existing algorithms. We conducted ablation studies where the significance of spatial and temporal measures on the overall performance were gauged.

Although the proposed method achieved state of the art performance, the highest correlation we achieved is around 0.8, which suggests that there is ample room for further improvement. For band-pass filtering we employed a simple Haar filter which has poor frequency response and can potentially limit the performance. As part of future work we wish to explore other band-pass filters with superior frequency response. Another avenue we wish to explore concerns the possibility of combining quality estimates from multiple temporal bands in a perceptually weighted manner with weights motivated by the temporal CSF. Also our proposed model can be incorporated in a data driven quality model such as VMAF [19] to further enhance the performance.

REFERENCES

- [1] [n.d.]. Acer Predator X27. <https://www.acer.com/ac/en/US/content/predator-series/predatorx27>. [Online; accessed 1-November-2019].
- [2] [n.d.]. Palette Gear console. <https://monogramcc.com>. [Online; accessed 1-November-2019].
- [3] 2019. GoPro Hero 8. <https://gopro.com/en/us/shop/hero8-black>. [Online; accessed 1-November-2019].
- [4] 2019. Sony RX series. <https://www.sony.com/electronics/compact-cameras/t/cyber-shot-digital-cameras>. [Online; accessed 1-November-2019].
- [5] Christos G Bampis, Praful Gupta, Rajiv Soundararajan, and Alan C Bovik. 2017. SpEED-QA: Spatial Efficient Entropic Differencing for Image and Video Quality. *IEEE Signal Processing Letters* 24, 9 (Sep. 2017), 1333–1337.
- [6] S Grace Chang, Bin Yu, and Martin Vetterli. 2000. Adaptive wavelet thresholding for image denoising and compression. *IEEE Transactions on Image Processing* 9, 9 (2000), 1532–1546.
- [7] Shyamprasad Chikkerur, Vijay Sundaram, Martin Reisslein, and Lina J Karam. 2011. Objective video quality assessment methods: A classification, review, and performance comparison. *IEEE Transactions on Broadcasting* 57, 2 (2011), 165–182.
- [8] Ronald R Coifman and M Victor Wickerhauser. 1992. Entropy-based algorithms for best basis selection. *IEEE Transactions on Information Theory* 38, 2 (1992), 713–718.
- [9] CVVP-3085-4K-8. [n.d.]. Clearview Player. <https://videoclarity.com/PDF/ClearView-Player-DataSheet.pdf>. [Online; accessed 1-November-2019].
- [10] Varuna De Silva, Hemantha Kodikara Arachchi, Erhan Ekmekcioglu, and Ahmet Kondoz. 2013. Toward an impairment metric for stereoscopic video: A full-reference video quality metric to assess compressed stereoscopic video. *IEEE Transactions on Image Processing* 22, 9 (2013), 3392–3404.
- [11] Minh N Do and Martin Vetterli. 2002. Wavelet-based texture retrieval using generalized Gaussian density and Kullback-Leibler distance. *IEEE Transactions on Image Processing* 11, 2 (2002), 146–158.
- [12] FFmpeg. [n.d.]. Encoding for streaming sites. <https://trac.ffmpeg.org/wiki>. [Online; accessed 1-November-2019].
- [13] Chang Ge, Ning Wang, Gerry Foster, and Mick Wilson. 2017. Toward QoE-assured 4K video-on-demand delivery through mobile edge virtualization with adaptive

prefetching. *IEEE Transactions on Multimedia* 19, 10 (2017), 2222–2237.

[14] ITU-R Recommendation BT.500-11. 2000. Methodology for the Subjective Assessment of the Quality of Television Pictures. *International Telecommunication Union* (2000).

[15] Woojae Kim, Jongyoo Kim, Sewoong Ahn, Jinwoo Kim, and Sanghoon Lee. 2018. Deep video quality assessor: From spatio-temporal visual sensitivity to a convolutional neural aggregation network. In *Proceedings of the European Conference on Computer Vision (ECCV)*. 219–234.

[16] Debarati Kundu, Deepthi Ghadiyaram, Alan C Bovik, and Brian L Evans. 2017. No-reference quality assessment of tone-mapped HDR pictures. *IEEE Transactions on Image Processing* 26, 6 (2017), 2957–2971.

[17] Qiang Li and Zhou Wang. 2009. Reduced-reference image quality assessment using divisive normalization-based image representation. *IEEE journal of selected topics in signal processing* 3, 2 (2009), 202–211.

[18] X. Li, Q. Guo, and X. Lu. 2016. Spatiotemporal Statistics for Video Quality Assessment. *IEEE Transactions on Image Processing* 25, 7 (July 2016), 3329–3342.

[19] Zhi Li, Anne Aaron, Ioannis Katsavounidis, Anush Moorthy, and Megha Manohara. 2016. Toward a practical perceptual video quality metric. “<http://techblog.netflix.com/2016/06/toward-practical-perceptual-video.html>”

[20] Alex Mackin, Fan Zhang, and David R Bull. 2018. A study of high frame rate video formats. *IEEE Transactions on Multimedia* 21, 6 (2018), 1499–1512.

[21] Zicong Mai, Hassan Mansour, Rafal Mantiuk, Panos Nasiopoulos, Rabab Ward, and Wolfgang Heidrich. 2010. Optimizing a tone curve for backward-compatible high dynamic range image and video compression. *IEEE Transactions on Image Processing* 20, 6 (2010), 1558–1571.

[22] K. Manasa and S. S. Channappayya. 2016. An Optical Flow-Based Full Reference Video Quality Assessment Algorithm. *IEEE Transactions on Image Processing* 25, 6 (June 2016), 2480–2492.

[23] Anish Mittal, Anush K. Moorthy, and Alan C Bovik. 2012. No-reference image quality assessment in the spatial domain. *IEEE Transactions on Image Processing* 21, 12 (Dec. 2012), 4695–4708.

[24] Anish Mittal, Rajiv Soundararajan, and Alan C Bovik. 2013. Making a “completely blind” image quality analyzer. *IEEE Signal Processing Letters* 20, 3 (March 2013), 209–212.

[25] D. Mukherjee, J. Han, J. Bankoski, R. Bultje, A. Grange, J. Koleszar, P. Wilkins, and Y. Xu. 2015. A Technical Overview of VP9™ The Latest Open-Source Video Codec. *SMPTE Motion Imaging Journal* 124, 1 (Jan 2015), 44–54.

[26] Rasoul Mohammadi Nasiri, Zhengfang Duanmu, and Zhou Wang. 2018. Temporal motion smoothness and the impact of frame rate variation on video quality. In *2018 25th IEEE International Conference on Image Processing (ICIP)*. IEEE, 1418–1422.

[27] Rasoul Mohammadi Nasiri, Jiheng Wang, Abdul Rehman, Shiqi Wang, and Zhou Wang. 2015. Perceptual quality assessment of high frame rate video. In *2015 IEEE 17th International Workshop on Multimedia Signal Processing (MMSP)*. IEEE, 1–6.

[28] Rasoul Mohammadi Nasiri and Zhou Wang. 2017. Perceptual aliasing factors and the impact of frame rate on video quality. In *2017 IEEE International Conference on Image Processing (ICIP)*. IEEE, 3475–3479.

[29] Xunyu Pan, Xing Zhang, and Siwei Lyu. 2012. Exposing image splicing with inconsistent local noise variances. In *2012 IEEE International Conference on Computational Photography (ICCP)*. IEEE, 1–10.

[30] John G Robson. 1966. Spatial and temporal contrast-sensitivity functions of the visual system. *Josa* 56, 8 (1966), 1141–1142.

[31] Daniel L Ruderman. 1994. The statistics of natural images. *Network: computation in neural systems* 5, 4 (1994), 517–548.

[32] Michele A Saad, Alan C Bovik, and Christophe Charrier. 2014. Blind Prediction of Natural Video Quality. *IEEE Transactions on Image Processing* 23, 3 (March 2014), 1352–1365.

[33] Kalpana Seshadrinathan and Alan C Bovik. 2010. Motion Tuned Spatio-Temporal Quality Assessment of Natural Videos. *IEEE Transactions on Image Processing* 19, 2 (Feb 2010), 335–350.

[34] Kalpana Seshadrinathan, Rajiv Soundararajan, Alan C Bovik, and Lawrence K Cormack. 2010. Study of Subjective and Objective Quality Assessment of Video. *IEEE Transactions on Image Processing* 19, 6 (June 2010), 1427–1441.

[35] Hamid R Sheikh and Alan C Bovik. 2006. Image Information and Visual Quality. *IEEE Trans. Image Process.* 15, 2 (Feb. 2006), 430–444.

[36] Aljoscha Smolic, Karsten Mueller, Nikolic Stefanoski, Joern Ostermann, Atanas Gotchev, Gozde B Akar, Georgios Triantafyllidis, and Alper Koz. 2007. Coding algorithms for 3DTV™ survey. *IEEE Transactions on Circuits and Systems for Video Technology* 17, 11 (2007), 1606–1621.

[37] Rajiv Soundararajan and Alan C Bovik. 2012. RRED Indices: Reduced Reference Entropic Differencing for Image Quality Assessment. *IEEE Transactions on Image Processing* 21, 2 (Feb. 2012), 517–526.

[38] Rajiv Soundararajan and Alan C Bovik. 2013. Video Quality Assessment by Reduced Reference Spatio-Temporal Entropic Differencing. *IEEE Transactions on Circuits and Systems for Video Technology* 23, 4 (April 2013), 684–694.

[39] Hamza Soury and Mohamed-Slim Alouini. 2015. New results on the sum of two generalized Gaussian random variables. In *2015 IEEE Global Conference on Signal and Information Processing (GlobalSIP)*. IEEE, 1017–1021.

[40] VQEG. 2000. Final report from the video quality experts group on the validation of objective quality metrics for video quality assessment.

[41] P. V. Vu, C. T. Vu, and D. M. Chandler. 2011. A spatiotemporal most-apparent-distortion model for video quality assessment. In *2011 18th IEEE International Conference on Image Processing*. 2505–2508.

[42] Martin J Wainwright and Eero P Simoncelli. 2000. Scale mixtures of Gaussians and the statistics of natural images. In *Advances in neural information processing systems*. 855–861.

[43] Zhou Wang and Alan C Bovik. 2009. Mean squared error: Love it or leave it? A new look at signal fidelity measures. *IEEE signal processing magazine* 26, 1 (2009), 98–117.

[44] Zhou Wang and Eero P Simoncelli. 2005. Reduced-reference image quality assessment using a wavelet-domain natural image statistic model. In *Human Vision and Electronic Imaging X*, Vol. 5666. International Society for Optics and Photonics, 149–159.

[45] Zhou Wang, Eero P Simoncelli, and Alan C Bovik. 2003. Multiscale structural similarity for image quality assessment. In *The Thirtieth Asilomar Conference on Signals, Systems Computers, 2003*, Vol. 2. 1398–1402 Vol.2.

[46] F. Zhang, A. Mackin, and D. R. Bull. 2017. A frame rate dependent video quality metric based on temporal wavelet decomposition and spatiotemporal pooling. In *2017 IEEE International Conference on Image Processing (ICIP)*. 300–304.

[47] Lin Zhang, Lei Zhang, Xuanqin Mou, and David Zhang. 2011. FSIM: A feature similarity index for image quality assessment. *IEEE Transactions on Image Processing* 20, 8 (2011), 2378–2386.

[48] Qian Zhao, Hong-wei Li, and Yuan-tong Shen. 2004. On the sum of generalized Gaussian random signals. In *Proceedings 7th International Conference on Signal Processing, 2004. Proceedings. ICSP'04. 2004*, Vol. 1. IEEE, 50–53.

[49] Zhou Wang, Alan C Bovik, Hamid R Sheikh, and Eero P Simoncelli. 2004. Image quality assessment: from error visibility to structural similarity. *IEEE Transactions on Image Processing* 13, 4 (April 2004), 600–612.